Review Article | Pediatric Imaging

https://doi.org/10.3348/kjr.2017.18.1.194
pISSN 1229-6929 · eISSN 2005-8330
Korean J Radiol 2017;18(1):194-207

Korean Journal of Radiology
KJR

Advanced MRI for Pediatric Brain Tumors with Emphasis on Clinical Benefits

Hyun Woo Goo, MD, PhD[1], Young-Shin Ra, MD, PhD[2]

[1]Department of Radiology and Research Institute of Radiology, Asan Medical Center, University of Ulsan College of Medicine, Seoul 05505, Korea; [2]Department of Neurosurgery, Asan Medical Center, University of Ulsan College of Medicine, Seoul 05505, Korea

Conventional anatomic brain MRI is often limited in evaluating pediatric brain tumors, the most common solid tumors and a leading cause of death in children. Advanced brain MRI techniques have great potential to improve diagnostic performance in children with brain tumors and overcome diagnostic pitfalls resulting from diverse tumor pathologies as well as nonspecific or overlapped imaging findings. Advanced MRI techniques used for evaluating pediatric brain tumors include diffusion-weighted imaging, diffusion tensor imaging, functional MRI, perfusion imaging, spectroscopy, susceptibility-weighted imaging, and chemical exchange saturation transfer imaging. Because pediatric brain tumors differ from adult counterparts in various aspects, MRI protocols should be designed to achieve maximal clinical benefits in pediatric brain tumors. In this study, we review advanced MRI techniques and interpretation algorithms for pediatric brain tumors.

Keywords: *Brain tumors; Imaging techniques; Infants and children; Pediatrics; Magnetic resonance imaging; Magnetic resonance spectroscopy; Diffusion-weighted imaging; Perfusion imaging*

INTRODUCTION

Brain tumors are the most common solid tumor and a leading cause of death in children (1). Evaluating pediatric brain tumors is often a diagnostic challenge due to their diverse tumor pathologies, nonspecific or overlapped imaging findings, recent evidence of gadolinium deposition in the brain, susceptibility artifacts from intratumoral calcification or hemorrhage, susceptibility artifacts related to tumor locations close to the skull base, and limited signal-to-noise ratios (SNRs) and motion artifacts in young children. The initial diagnosis of pediatric brain tumors is almost always based on patient age, tumor location, and neuroimaging findings. Beside the initial diagnosis, other goals of brain MRI for pediatric brain tumors should include differentiation of specific tumor types, grading tumors, distinguishing viable tumor from necrotic tissue, guiding stereotactic biopsy, and determining treatment responses (2, 3). As conventional anatomic brain MRI is often limited in achieving these goals, advanced MRI techniques, such as diffusion-weighted imaging (DWI), diffusion tensor imaging (DTI), functional MRI, perfusion imaging, MR spectroscopy (MRS), and susceptibility-weighted imaging (SWI), are commonly included in the MRI protocol (2-9). The recently introduced chemical exchange saturation transfer (CEST) imaging is at the early stage of clinical investigations (10). Regarding field strengths of MRI systems, 3T is the current standard of neuroimaging mainly due to higher contrast-to-noise ratio and SNR (11). In this article, we review advanced MRI techniques and findings in pediatric brain tumors, with particular emphasis on how to utilize diagnostic clues to maximize clinical benefits, which will

Received March 12, 2016; accepted after revision August 17, 2016.
Corresponding author: Hyun Woo Goo, MD, Department of Radiology and Research Institute of Radiology, Asan Medical Center, University of Ulsan College of Medicine, 88 Olympic-ro 43-gil, Songpa-gu, Seoul 05505, Korea.
• Tel: (822) 3010-4388 • Fax: (822) 476-0090
• E-mail: hwgoo@amc.seoul.kr

Korean Journal of Radiology
KJR

ultimately improve patient outcome.

Diffusion-Weighted Imaging

Diffusion-weighted imaging provides qualitative and quantitative assessments of water diffusion in brain tumors, reflecting tumor cellularity. To avoid the so-called T2-shine-through effects possibly leading to false positive diagnosis on DWI, whether a hyperintense area on DWI also shows restricted water diffusion (hypointensity) on the apparent diffusion coefficient (ADC) map should be confirmed. Low ADC values in pediatric brain tumors generally suggest high-grade hypercellular tumors, such as medulloblastoma, primitive neuroectodermal tumor, and glioblastoma, whereas low-grade gliomas usually show high ADC values. However, considerable overlap of ADC values between high- and low-grade tumors in both pediatric and adult patients results in limited clinical value of DWI for tumor grading (12, 13). In addition, ADC values are affected by the presence of intratumoral hemorrhage and calcification frequently included in pediatric brain tumors.

Apparent diffusion coefficient values are calculated by using 2 b-values, most commonly 0 and 1000 s/mm^2, and a monoexponential model. However, the ADC values do not accurately indicate pure water diffusion in the tissue and tend to be overestimated because they are contaminated by perfusion most apparent in low b-values (e.g., < 100–150 s/mm^2). Recent studies reported that ADC ratios,

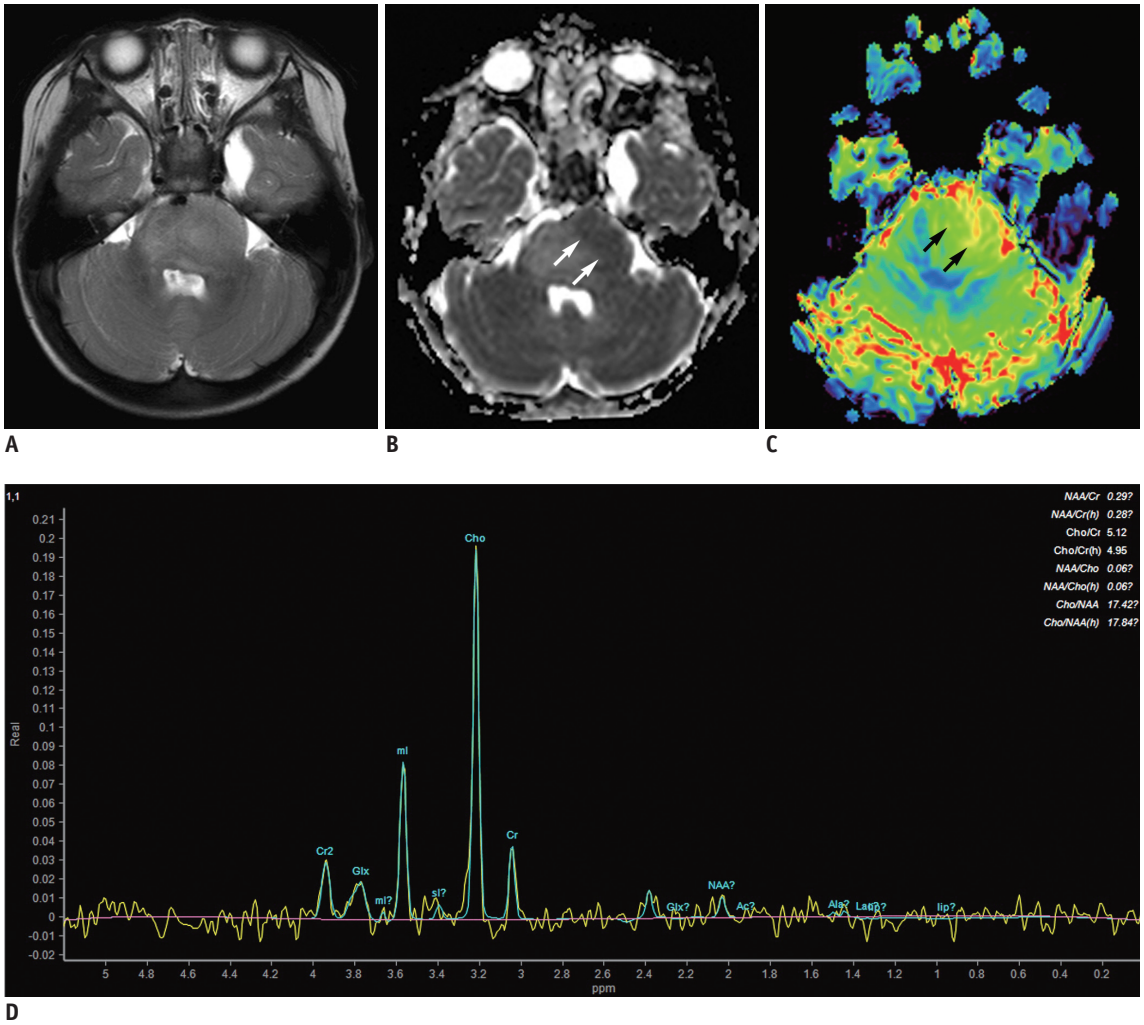

Fig. 1. 3-year-old boy with anaplastic astrocytoma (WHO grade III).
A. Axial T2-weighted image shows diffuse pontine tumor with eccentric bulging on left side. **B.** Axial apparent diffusion coefficient map reveals region with restricted diffusion (arrows) suggesting higher-grade tumor on anterolateral portion of left pons. **C.** Axial cerebral blood volume map from dynamic susceptibility contrast imaging demonstrates that same region (arrows) also shows increased tumor perfusion. Substantial image distortion is noted along skull base. **D.** Single-voxel intermediate echo time (144 ms) MR spectroscopy obtained in region shows exceedingly high choline/creatine ratio strongly suggesting high-grade tumor. WHO = World Health Organization

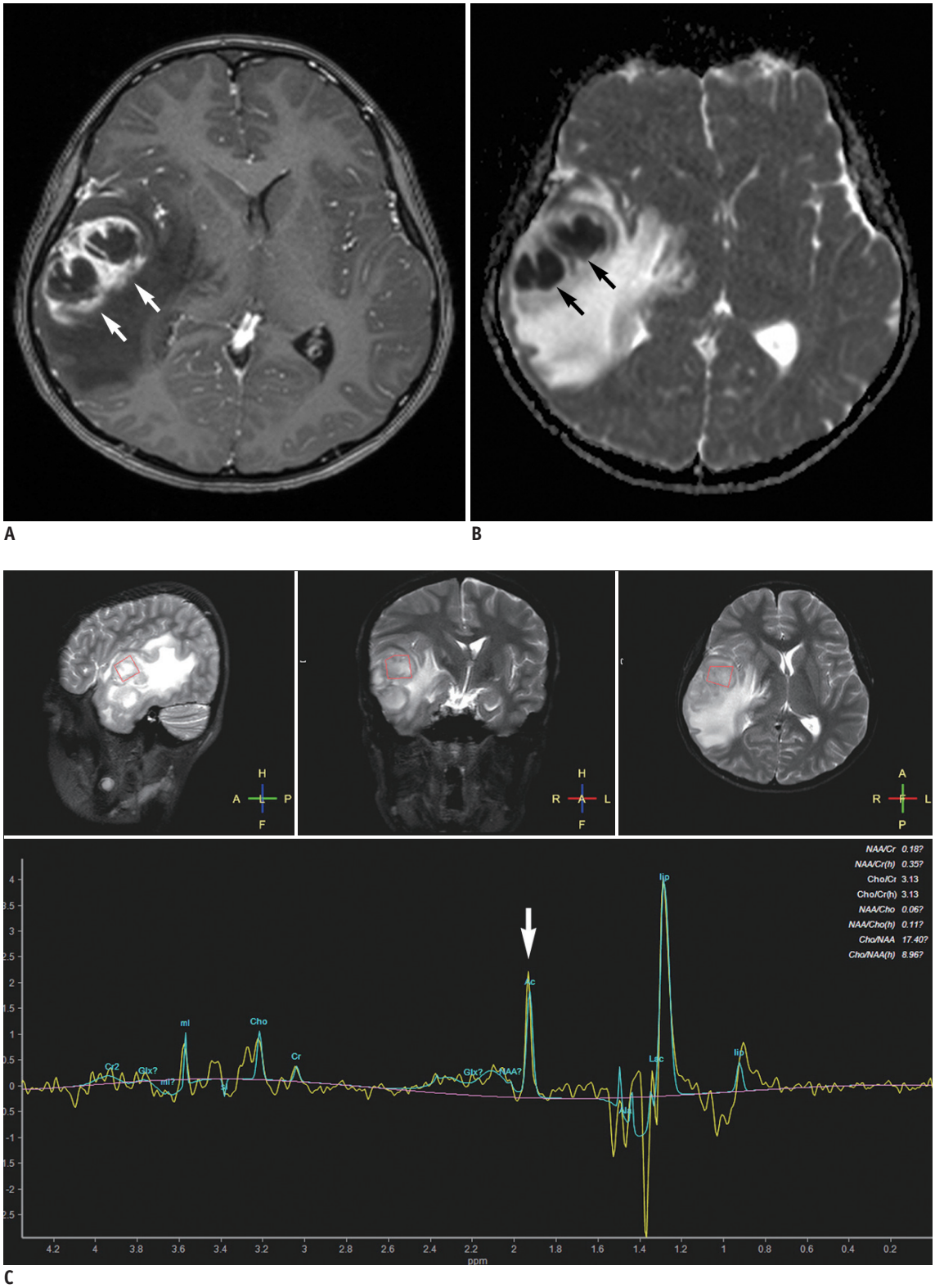

Fig. 2. 11-year-old boy with pyogenic abscess.
A. Axial enhanced T1-weighted image irregular rim-enhancing lesion (arrows) with extensive perilesional edema in right temporo-parietal area. **B.** On axial apparent diffusion coefficient map, central non-enhancing portions show restricted diffusion (arrows) suggesting pyogenic abscess. Water diffusion should increase in tumor necrosis. **C.** Single-voxel intermediate echo time (144 ms) MR spectroscopy demonstrates acetate peak (arrow) approximately at 1.9 ppm and amino acids (including alanine approximately at 1.5 ppm)/lipid/lactate peaks strongly suggesting pyogenic abscess.

Korean Journal of Radiology
KJR

histogram analysis, and diffusion kurtosis based on non-Gaussian water diffusion might better characterize high-grade brain tumors (3, 14-16). Furthermore, a diffusion heterogeneity index calculated from a stretched exponential model or a fractional order calculus model with multi-b-value DWI recently demonstrates improved tumor grading in adult gliomas (16) and pediatric brain tumors (17). In 67 pediatric patients with brain tumors, fractional order calculus model parameters, such as diffusion coefficient, fractional order parameter, and a microstructural quantity, are used to improve differentiation between low- and high-grade pediatric brain tumor groups with a high predictive power (area under curve, 0.962) and accuracy (92.5%) at the expense of longer acquisition time (17).

Diffusion-weighted imaging is particularly useful to identify a high-grade component in brainstem tumors to place single-voxel MRS as well as determine stereotactic biopsy site (Fig. 1). In our institution, stereotactic biopsy is actively performed in brainstem tumors to obtain accurate pathologic diagnosis crucial for appropriate treatment with high diagnostic yield and safety profile. DWI can also be used to differentiate tumor mimics from true tumors, for example, pyogenic abscess from necrotic tumor (Fig. 2). In high-grade tumors with low ADC values, DWI may be used to evaluate treatment responses and detect early tumor recurrence.

Single-shot spin-echo echo-planar imaging sequence has been a standard for DWI, but substantial image distortion and susceptibility artifact may hamper image interpretation because pediatric brain tumors are often adjacent to the skull base. To overcome this diagnostic challenge, alterative pulse sequence, such as single-shot turbo-spin-echo sequence, multi-shot echo-planar imaging sequence, radial k-space sampling technique, or DWI with background body signal suppression (11), can be used (Fig. 3).

Diffusion Tensor Imaging

In contrast to DWI, DTI with at least 6 diffusion-sensitizing gradient directions provides anisotropic water diffusion in the brain mostly caused by the white matter tracts. The degree and the direction of the anisotropic water diffusion are demonstrated by fractional anisotropy (FA) map and color-coded map. Tumor infiltration in peritumoral edema may be delineated exclusively on DTI but not on other MRI techniques (18, 19). Fiber tractography

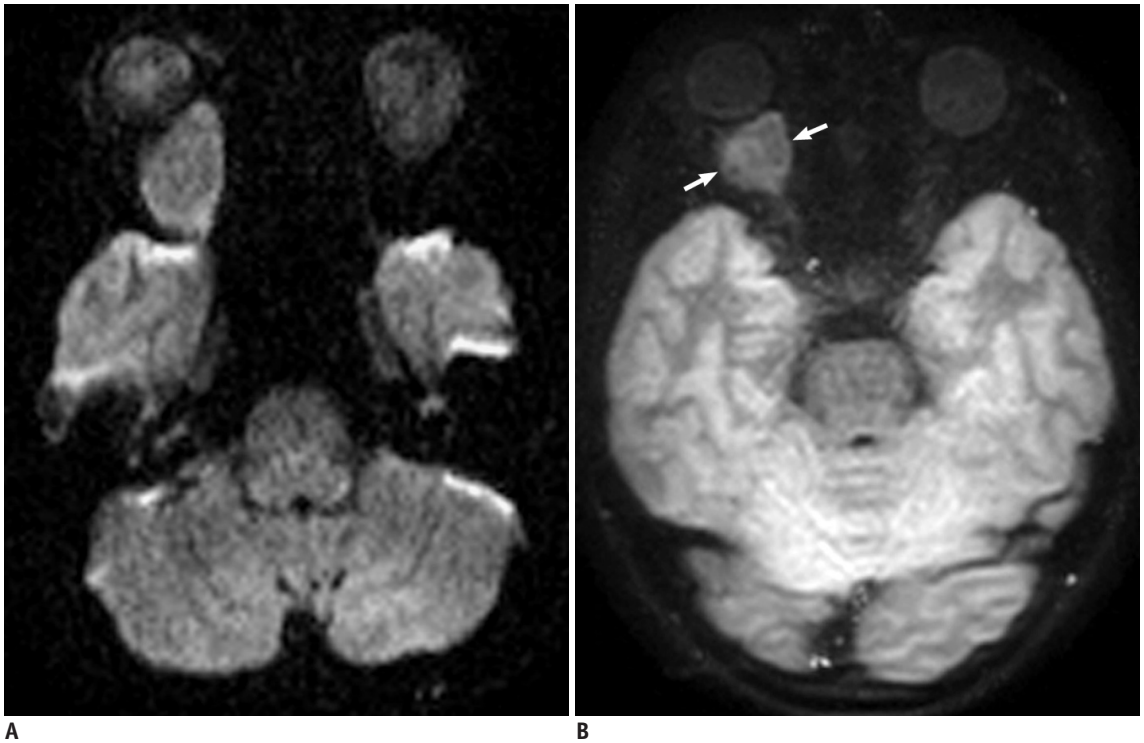

Fig. 3. 14-year-old girl with right optic nerve sheath meningioma.
Compared with axial diffusion-weighted image using single-shot spin-echo echo-planar sequence **(A)**, image distortion is considerably reduced on axial diffusion-weighted image using single-shot turbo-spin-echo sequence **(B)**. As result, right orbital tumor (arrows) is better delineated without image distortion on turbo-spin-echo diffusion-weighted image **(B)**.

reconstructed from DTI data is essential for surgical planning, particularly in brainstem and supratentorial tumors, by illustrating spatial relationships between major functional fibers, such as motor, language, and visual tracts, and brain tumors (Fig. 4) (8, 9, 18-21). However, diagnostic pitfalls of fiber tractography caused by crossing fibers, false negative findings, image distortion due to magnetic susceptibility artifacts, and intraoperative brain shifting, should be considered to avoid misinterpretation (20). In addition, FA values are potentially useful for evaluating radiation-induced white matter injury in pediatric brain tumors (8, 9). Compared with healthy age-matched control subjects, FA values are reduced in children who are treated for medulloblastoma and reduction of supratentorial white matter FA values in these patients correlates with younger age at treatment, longer interval since treatment, and deterioration of school performance (22).

Functional MRI

In addition to fiber tractography, functional MRI using blood oxygen level-dependent technique may be used to localize eloquent cortical gray matter to minimize postsurgical neurological deficits (23). However, reliable results may be difficult in young children since successful functional MRI is cooperation-dependent (24). In

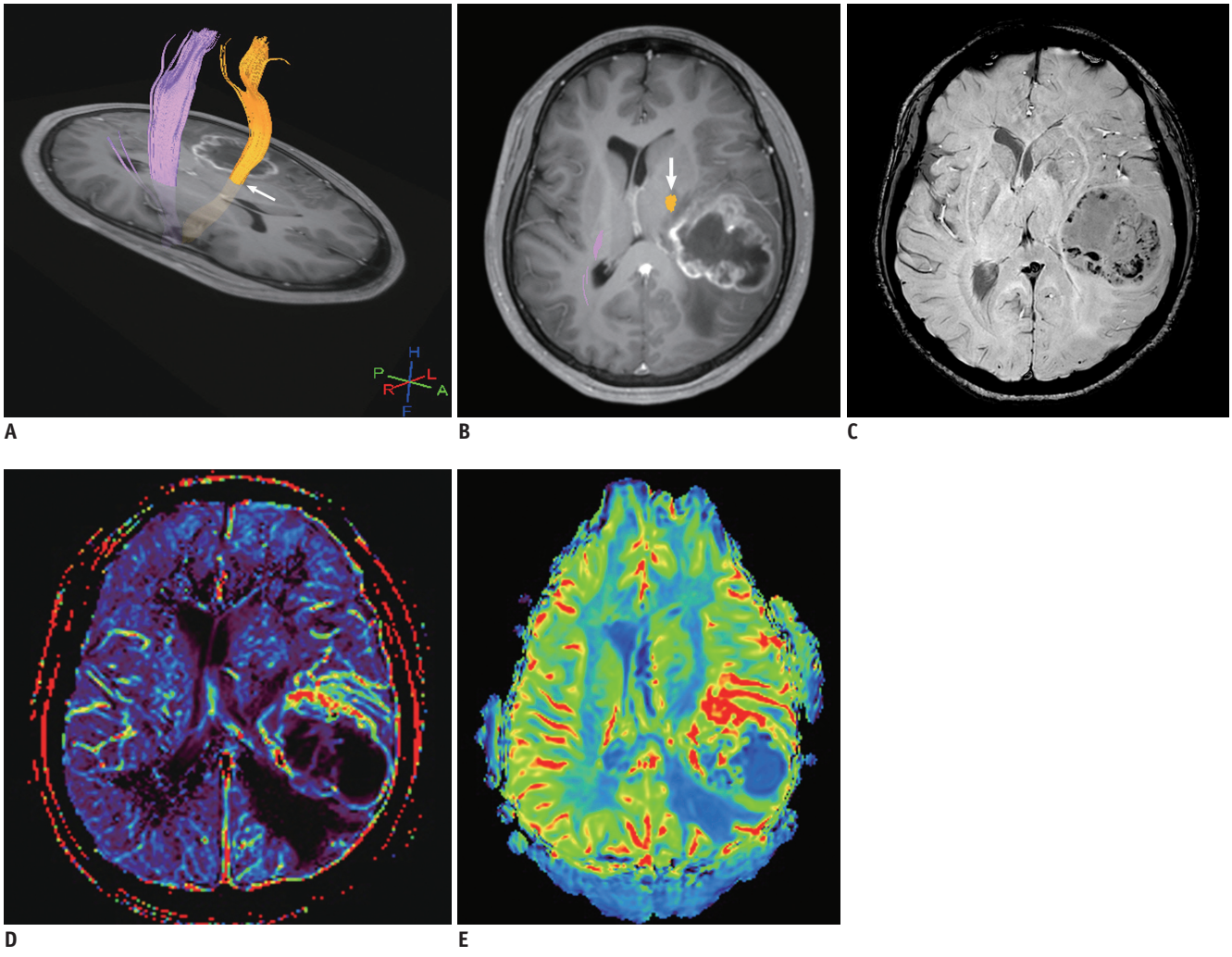

A B C D E

Fig. 4. 15-year-old girl with anaplastic ependymoma.
Three-dimensional **(A)** and two-dimensional **(B)** fiber tractographies illustrate that left corticospinal motor fibers (arrows) are intact and displaced anteromedially by heterogeneously enhancing necrotic tumor. Axial susceptibility-weighted image reveals multiple hypointense foci predominantly in peripheral portion of tumor indicating hemorrhage or neovascularity **(C)**. K_{trans} map **(D)** and cerebral blood volume map from dynamic susceptibility contrast imaging **(E)** show increased values only in anterior and medial peripheral portions of tumor. Therefore, hypointense foci in posterior and lateral portions of tumor on susceptibility-weighted image mainly represent hemorrhagic necrosis. Image distortion on dynamic susceptibility contrast image is pronounced in anterior part of brain **(E)**.

Korean Journal of Radiology
KJR

uncooperative patients, passive range of motion or resting-state may be used as an alternative of task-based functional MRI (25, 26). Functional MRI is helpful in selecting patients in whom a functional area is adjacent to or within the tumor requiring intraoperative cortical stimulation (9).

Perfusion Imaging

Perfusion MRI providing the degree of neovascularity or tumor angiogenesis at tissue level is useful for tumor grading and prognostication (6, 27). Three types of perfusion MRI techniques include dynamic susceptibility contrast (DSC) imaging, dynamic contrast-enhanced (DCE) imaging, and arterial spin labeling (ASL) imaging. An exogenous contrast agent is used in DSC imaging and DCE imaging, while no exogenous contrast agent is necessary in ASL imaging. DSC imaging is the standard perfusion MRI method that is widely used in brain tumors, while DCE imaging is regarded as a viable alternative. ASL imaging, especially promising in children, is still evolving and improving to gain more clinical acceptance. The technical feasibility of dual contrast perfusion MRI, comprising an ultrasmall superparamagnetic iron oxide contrast agent-enhanced DSC imaging and a gadolinium-based contrast agent-enhanced DCE imaging, in a single imaging session was reported in 7 patients with pediatric brain tumors (28). However, the advantage of such dual contrast perfusion MRI in pediatric brain tumors is not proven and fast injection of an ultrasmall superparamagnetic iron oxide contrast agent may not be safe. In addition, there is a growing concern of gadolinium accumulation in the brain, such as the dentate nucleus and globus pallidus, in patients with normal renal function following multiple gadolinium-based contrast-enhanced MRI examinations (29, 30). As in nephrogenic systemic fibrosis, the macrocyclic gadolinium chelates are more stable and, therefore, less accumulated in the brain than the linear chelates. Although the clinical significance of this gadolinium deposition remains to be elucidated, contrast-enhanced perfusion MRI, such as DSC and DCE, should be carefully performed in children with brain tumors. A macrocyclic gadolinium-based rather than a linear contrast agent, has been intravenously administered for contrast-enhanced pediatric MRI examinations in our institution since 2007. In this regard, non-contrast perfusion MRI, such as ASL imaging, is a valuable alternative to contrast-enhanced perfusion MRI, particularly in children.

Dynamic Susceptibility-Weighted Contrast-Enhanced Imaging

Signals at DSC imaging using a dynamic T2*-weighted gradient-echo echo-planar imaging are derived from the T2* susceptibility effect (negative enhancement) caused by intravenously injected gadolinium contrast agent. Perfusion parameters including relative cerebral blood volume (rCBV), relative cerebral blood flow (rCBF), and mean transit time (MTT) are calculated by using various methods, such as the indicator dilution method and the pharmacokinetic modeling approach. In general, rCBV values are most commonly reported because of the intricacies in measuring absolute arterial input function (27).

In 63 pediatric brain tumors, rCBV values from DSC imaging showed considerable overlap between low-grade and high-grade tumors, particularly between pilocytic astrocytoma and medulloblastoma (31). It is suggested that high negative predictive value (88% at maximum rCBV of 1.38) of DSC imaging may be used to exclude high-grade tumors in selective patients whose conventional imaging is inconclusive (31). In addition, maximum rCBV values (the highest CBV value in tumor tissue divided by the CBV value in normal-appearing contralateral white matter) have potential in differentiating atypical teratoid rhabdoid tumor (6.9 ± 0.8) from medulloblastoma (3.8 ± 1.7) (t = 2.98, p = 0.01) (31). Similarly, hemangioblastoma showing exceedingly high rCBV values can be differentiated from pilocytic astrocytoma, while they are often indistinguishable based on conventional MRI alone (8, 32). Relatively high rCBV values may be seen in low-grade tumors, such

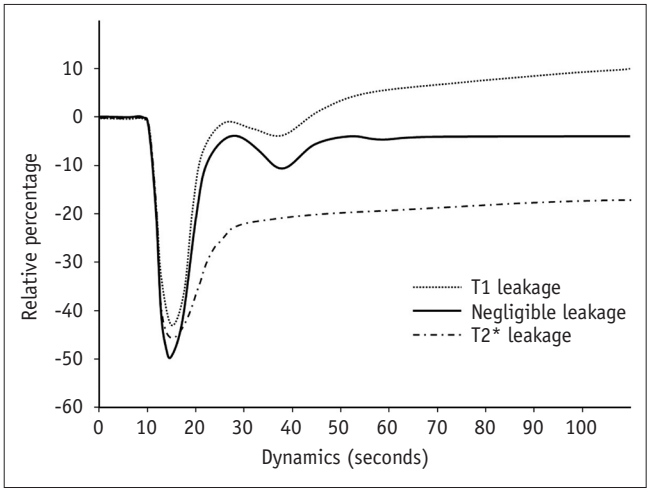

Fig. 5. Signal intensity-time curve of dynamic susceptibility contrast imaging. Curve of T1-dominant leakage pattern shows gradual increase above baseline at later dynamics, while curve of T2*-dominant leakage pattern fails to return to baseline.

as pilocytic astrocytoma, pilomyxoid astrocytoma, and oligodendroglioma (9, 29). DSC imaging is also helpful in distinguishing viable tumor from radiation necrosis and in differentiating true progression from pseudoprogression (3). Moreover, DSC imaging is particularly helpful to monitor antiangiogenic therapy (3). As in a focal area of restricted diffusion on ADC map, a high-grade subset in brainstem glioma may be presented as a focal area of high rCBV on DSC imaging (Fig. 1) (8).

Contrast leakage through disrupted blood-brain barrier in brain tumors violates the assumption that the injected contrast agent remains within the intravascular compartment during DSC imaging (4, 27). This contrast leakage with either T1 (above baseline) or T2* (failing to return to baseline) pattern (Fig. 5) requires appropriate correction, such as small preload dose (0.025–0.05 mmoL/

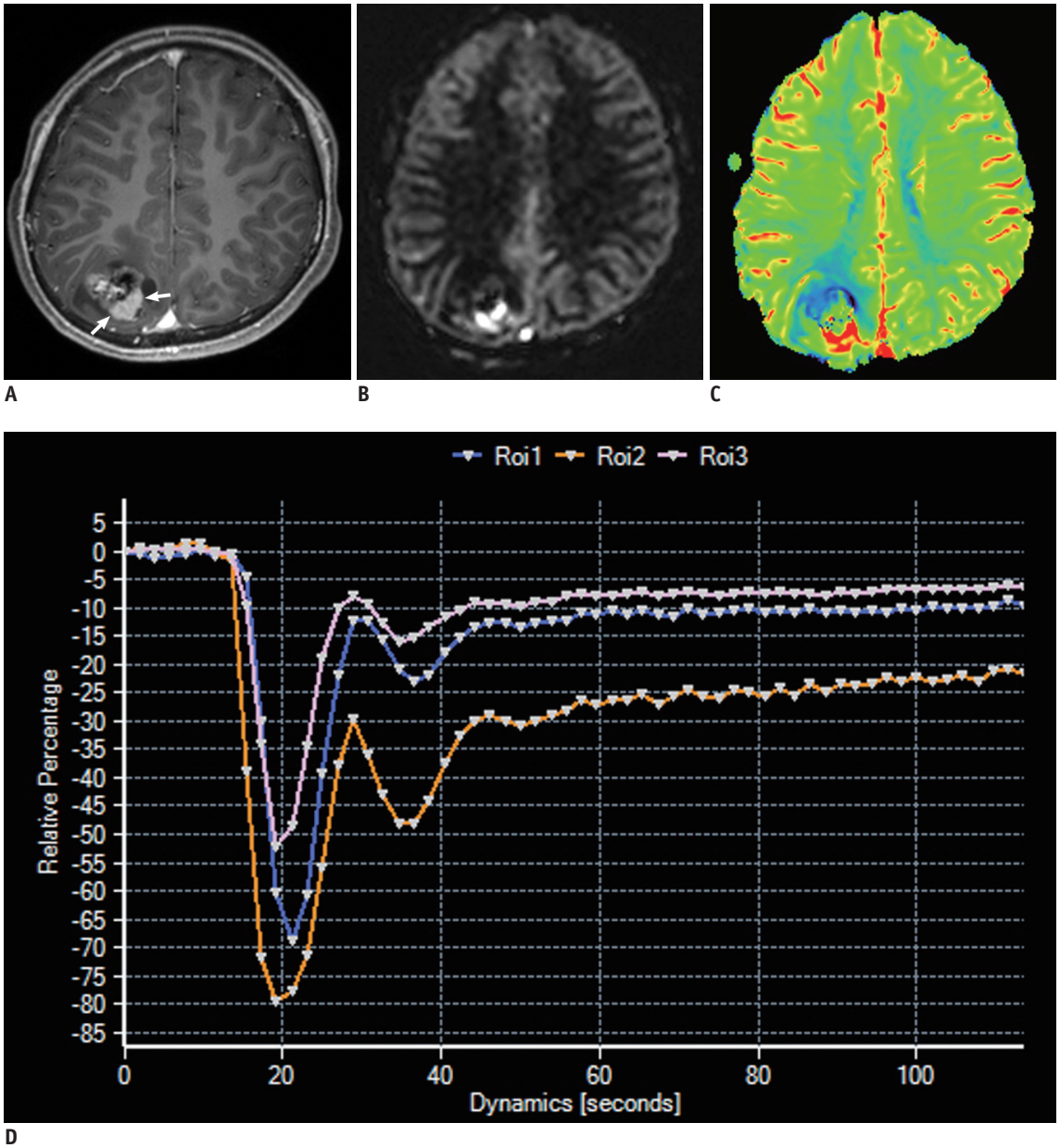

Fig. 6. 13-year-old boy with clear cell ependymoma (WHO grade II).
A. Axial enhanced T1-weighted image shows heterogeneous solid and cystic tumor with small enhancing portion (arrows) and mild peritumoral edema in peripheral portion of right parietal lobe. **B, C.** Axial pseudocontinuous arterial spinal labeling image **(B)** and cerebral blood flow map from dynamic susceptibility imaging **(C)** reveal increased values in enhancing tumor. **D.** Signal intensity-time curve of dynamic susceptibility contrast imaging demonstrates T2*-dominant leakage pattern for enhancing tumor showing increased tumor blood flow (region of interest 2), compared with normal-appearing brain regions (regions of interest 1 and 3). WHO = World Health Organization

Korean Journal of Radiology
KJR

kg) of a gadolinium contrast agent or posthoc leakage-correction algorithms, to obtain correct perfusion values from DSC imaging (7, 27). Ho et al. (33) reported that time-intensity curves of DSC imaging could be categorized into T1-dominant leakage pattern (n = 25), T2*-dominant leakage pattern (n = 15), and return to baseline (n = 23; ± 10% range) in 63 pediatric brain tumors. They also reported that T1-dominant leakage pattern was highly specific for a low-grade tumor, such as pilocytic or pilomyxoid astrocytoma. In contrast, T2*-dominant leakage pattern with markedly elevated rCBV may be seen in ependymoma (Fig. 6) and other high-grade tumors, which is attributed to the fenestrated blood vessels in the tumor (8).

Compared with adult patients, DSC imaging requiring high-flow contrast injection is technically challenging in children. Bolus delay and dispersion caused by slow injection rates leads to underestimation of CBF values and overestimation of MTT values. DSC imaging may not provide relevant perfusion values in brain tumors adjacent to the skull base that are common in children, because the imaging technique is extremely vulnerable to image distortion and susceptibility artifacts from brain-bone-air interfaces (Figs. 1, 4), blood products, and calcium (7).

Dynamic Contrast-Enhanced Imaging

Dynamic contrast-enhanced imaging using a T1-weighted gradient echo imaging (positive enhancement) provides quantitative hemodynamic indices, such as the transfer constant (K_{trans}) (Fig. 4), the rate constant, the extracellular extravascular space fractional volume, and the fractional plasma volume (V_p) (6, 21). In general, high-grade gliomas tend to have higher K_{trans} than low-grade gliomas in adult patients. Of interest, a case of childhood hemangioblastoma demonstrated characteristically low K_{trans} and high V_p values (34). However, further clinical evidence is needed to clarify its clinical value in pediatric brain tumors. DCE imaging is at least less problematic in image distortion and artifacts than DSC imaging, whereas DCE imaging is currently limited by shorter imaging coverage and lower temporal resolution. Dynamic data collection > 5 minutes is usually recommended in adult patients for adequate pharmacokinetic analysis of DCE imaging (27). Considering a shorter circulation time and transit time of injected contrast agent in children than in adults, the dynamic data collection time < 5 minutes may be relevant for pediatric patients.

Arterial Spin Labeling Imaging

Arterial spin labeling using endogenous arterial water as a diffusible tracer has several advantages in children including no use of exogenous contrast agent, high SNR, high labeling efficiency, and capability of repeated scans. ASL imaging techniques may be categorized into 4 types including pulsed ASL, continuous ASL, pseudocontinuous ASL, and velocity-selective ASL. For neurooncologic imaging, pseudocontinuous ASL is widely used because of its relatively higher SNR and greater tagging efficiency (Fig. 6). Potential for CBF quantification is regarded as a great advantage of ASL imaging over other perfusion imaging methods. However, CBF values from ASL imaging tend to be underestimated in brain regions with delayed flow, such as the white matter, and in tumor regions with tortuous vasculature. Conversely, CBF values are overestimated in regions with vascular shunts. A single compartment model is usually used for flow quantification of ASL imaging (27). Despite attempts to use two-stage model of ASL imaging with multiple inversion times for assessment of tumor perfusion and vascular structural abnormalities in 8 children with brain tumors (35), the complexity of this sophisticated model limits its clinical application.

In 30 adult patients with brain tumors, a positive linear correlation was found between regional DSC and ASL measurements of CBF, but a statistically significant voxel-wise correlation occurs in merely 30–40% of the patients (36). In addition, ASL imaging appears inferior to DSC imaging in differentiating World Health Organization (WHO) grades, particularly between grades III and IV (36). In 54 children with brain tumors, maximal rCBF values from ASL imaging were significantly higher in high-grade tumors (2.98 ± 1.90) than in low-grade tumors (1.12 ± 0.36), but a specific tumor type could not be differentiated based on these values (37). Of note, maximal rCBF values (1.05 ± 0.18) of pilocytic astrocytoma, a benign vascular tumor, are similar to those of contralateral gray matter, possibly due to the characteristic intratumoral capillary exchange rate (37). Similar to DSC imaging, rCBF value of hemangioblastoma measured by ASL imaging was extremely high (11.8) in a child (34), which is particularly helpful in differentiating hemangioblastoma from pilocytic astrocytoma. Thus, ASL imaging showing fewer susceptibility artifacts than DSC imaging may be beneficial for evaluating pediatric brain tumors adjacent to the skull base.

MR Spectroscopy

Proton MRS is divided into single-voxel and multi-voxel (MR spectroscopic imaging) methods depending on the number of voxels used for MRS, and into short (20–40 ms), intermediate (135–144 ms), and long echo time (270–280 ms) methods depending on echo times. Single-voxel method is generally used in clinical practice because multi-voxel method shows limited spectroscopic quality and spatial resolution. Nevertheless, multi-voxel method may be used to identify higher grade regions within large, heterogeneous tumors for biopsy targets. Longer echo time methods demonstrate fewer metabolites with long T2 relaxation times, such as N-acetylaspartate (NAA), choline (Cho), and creatine (Cr), as compared to short echo time method, but the baseline tends to be less fluctuating with longer echo time methods. An inverted doublet at 1.3 ppm at echo time of 144 ms is useful to identify a lactate peak. Compared with longer echo time methods, short echo time method allows the detection of additional metabolites, including

A B

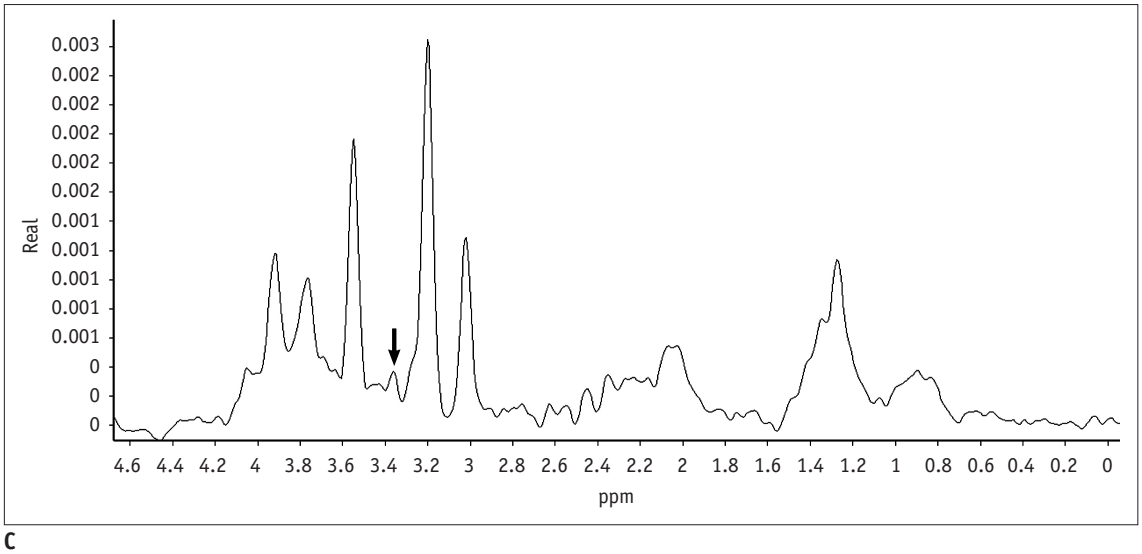

C

Fig. 7. 12-year-old boy with medulloblastoma.
A, B. Sagittal fluid-attenuated inversion recovery image **(A)** and axial enhanced T1-weighted image **(B)** show lobulated solid tumor probably originating from inferior cerebellar vermis and extruding through foramen of Magendie (arrow). Obstructed hydrocephalus by tumor is noted **(A)**. **C.** Single-voxel short echo time (40 ms) MR spectroscopy demonstrates small taurine peak (arrow), high choline/creatine ratio, and increased lipid/lactate peaks, strongly suggesting medulloblastoma.

Korean Journal of Radiology
KJR

taurine (Tau), glutamine plus glutamate, myoinositol (mI) plus glycine, and alanine (Ala), that occasionally give a diagnostic hint to a specific tumor type (38). The pulse sequences used for MRS include point resolved spectroscopy (PRESS) and stimulated echo acquisition method (STEAM). In general, the signal of PRESS is greater than that of STEAM and STEAM is more sensitive to motion.

Chief metabolites on MRS include NAA (a neuronal marker), Cho (a marker of active membrane turnover), Cr (an energy metabolism marker), mI (a glial marker), and lactate (a marker of anaerobic glycolysis), and each metabolite is identified at a specific ppm. The hallmark of MRS findings of brain tumors is elevated Cho and decreased NAA levels, often presented with metabolite ratios, such as Cho/Cr and NAA/Cr ratios. High-grade tumors usually have higher Cho/Cr and lower NAA/Cr ratios than low-grade tumors (Fig. 1). Lactate/lipid peaks reflect necrotic high-grade tumors. However, the MRS pattern suggesting high-grade tumors is typically seen in pilocytic astrocytoma (WHO grade I) (37). MRS has potential to differentiate between different type of pediatric brain tumors according to their different metabolites (2, 4, 39). Adding MRS to conventional MRI significantly improved diagnostic accuracy according to a study on 120 children with brain tumors (40).

A couple of metabolites are highly suggestive of specific tumor types. Tau at 3.3–3.4 ppm, one such metabolite, is useful to distinguish medulloblastoma (Fig. 7) from other pediatric cerebellar tumors if present. Tau may also be detected in pediatric supratentorial primitive neuroectodermal tumor (9). Elevated mI levels strongly suggest a diagnosis of grade II astrocytoma, ependymoma, or choroid plexus papilloma (38). A citrate peak approximately at 2.6 ppm in brainstem glioma, if identified, can be used to follow up the tumor because reduction of the peak may indicate malignant transformation or may be related to therapies, indicating that MRS may also be used to identify tumor progression and assess treatment responses of brain tumors (38). In diffuse pontine glioma, MRS can identify tumor progression or recurrence several months before clinical worsening (38). Elevated lipid peaks, low NAA peak, and low Cho peak are typically seen in radiation necrosis (38). Elevated Ala peak approximately at 1.4 ppm may be detected in meningioma, glioblastoma, and medulloblastoma (38). MRS may be used to differentiate non-tumorous benign lesions from brain tumors. For instance, the presence of acetate, succinate, and amino acids in the lesion center highly suggest a diagnosis of pyogenic abscess (Fig. 2) (38). Automatic identification of metabolites is now commonly used in clinical practice. However, misidentification of a metabolite as an adjacent common metabolite should be avoided (e.g., acetate as NAA, Ala as lactate), since it may lead to misinterpretation of entire MRS findings.

Susceptibility-Weighted Imaging

Susceptibility-weighted imaging accentuates the

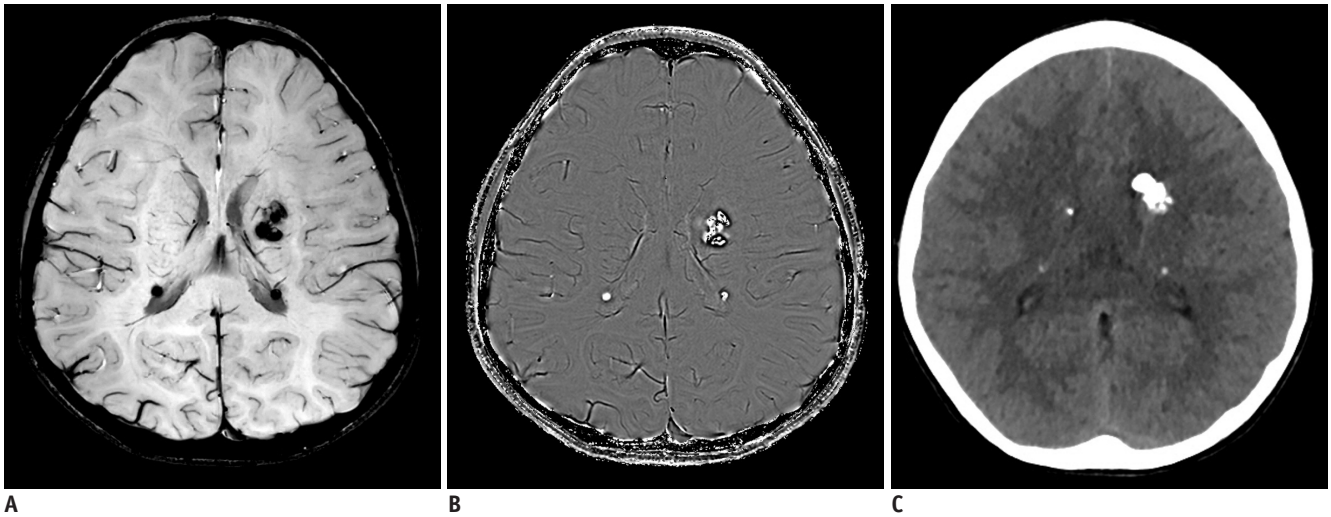

A B C

Fig. 8. 11-year-old boy with tuberous sclerosis.
Multiple calcified subependymal nodules appear hypointense and hyperintense on magnitude **(A)** and phase **(B)** images of susceptibility-weighted imaging, respectively, which is confirmed by precontrast brain CT **(C)**. In tuberous sclerosis, subependymal giant cell astrocytoma (WHO grade I), characterized by large subependymal mass (> 1 cm) near foramen of Monro showing calcifications, heterogeneous MRI signal intensity, and marked contrast enhancement, may cause obstructive hydrocephalus. WHO = World Health Organization

visualization of microvasculature and substances with magnetic susceptibilities, such as paramagnetic blood products and diamagnetic calcium, in brain tumors. Calcification (Fig. 8), typical of low-grade tumors, can be distinguished from hemorrhage or neovascularity (Fig. 2), typical of high-grade tumors, based on signal difference between magnitude and phase images of SWI or by using quantitative susceptibility mapping (41-43).

Potential value of SWI in tumor grading in adults has been reported by using various evaluation methods, such as intratumoral susceptibility signals, hypointensity ratios, and a computational fractal-based method (43). In addition, treatment response can be predicted or monitored based on SWI findings in adult tumors (43). However, more studies to refine the clinical value of SWI in pediatric brain tumors are required.

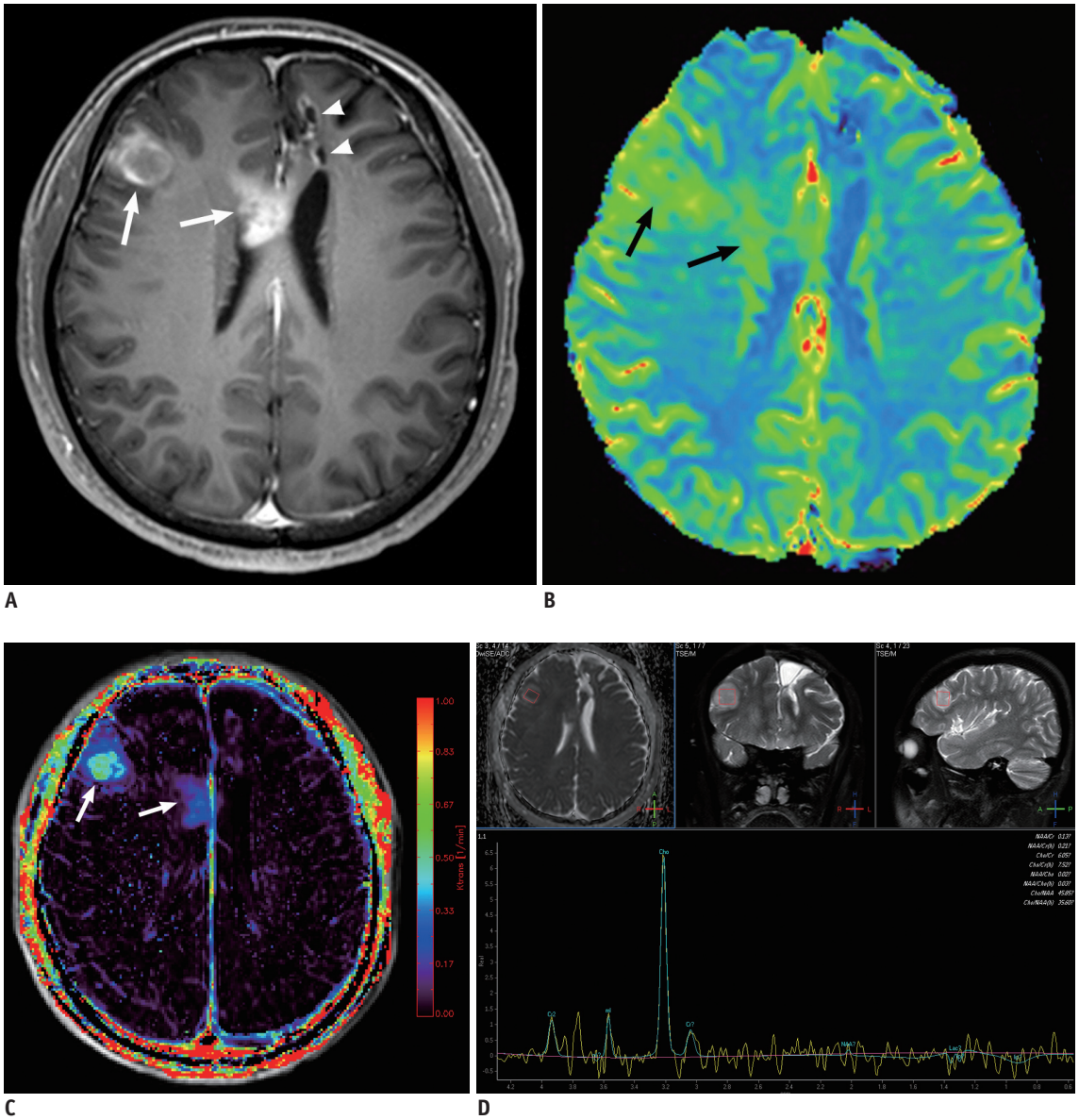

Fig. 9. 15-year-old boy with anaplastic oligodendroglioma who underwent intensity-modulated radiation therapy and chemotherapy after tumor resection.
A. Axial enhanced T1-weighted image shows irregular rim-enhancing lesions at previous tumor resection site in left frontal lobe (arrowheads) and newly developed enhancing lesions in right frontal lobe (arrow) and anterior corpus callosum (arrow). **B, C.** Cerebral blood volume map from dynamic susceptibility contrast imaging **(B)** and K_{trans} map **(C)** demonstrate increased tumor perfusion and vascular permeability in lesions (arrows), respectively. **D.** Single-voxel intermediate echo time (144 ms) MR spectroscopy acquired in right frontal lesion reveals highly increased Cho/Cr ratio and no discernible NAA peak. These two enhancing lesions were confirmed as recurred tumors rather than radiation necrosis. Cho = choline, Cr = creatine, NAA = N-acetylaspartate

Korean Journal of Radiology
KJR

Chemical Exchange Saturation Transfer Imaging

Chemical exchange saturation transfer imaging offers a new type of molecule specific contrast by detecting endogenous mobile proteins and peptides (10). Amide proton transfer (APT) imaging, one of CEST imaging methods, is used for brain tumors in which the intracellular exchangeable amide proton content increases. As a result, APT imaging may allow better identification of tumor boundaries, differentiation between glioma and radiation necrosis, and prediction of tumor response to therapy (10). In 36 adult patients with diffuse glioma, APT imaging could differentiate high-grade gliomas (3.8 ± 1.0%) from low-grade gliomas (2.1 ± 0.4%), with 93% sensitivity and 100% specificity (44). In orthotopic mouse model of glioblastoma, APT imaging could detect early therapeutic response to temozolomide (45). Increment of APT signal intensity in brain tumors is merely in the range of 2–4%. In general, the normalized APT signal intensity by the contralateral normal appearing white matter is used because its signal intensity is influenced by various conditions, including tissue water content, pH, temperature, the T1 of water, and the background magnetization transfer effect (44). Initial clinical applications of APT imaging to pediatric brain tumors are under investigation. Although technically feasible, APT imaging needs further improvement especially for shorter acquisition time and longer scan coverage to widen its clinical use.

Suggested Protocols for Pre-Treatment Evaluation and Post-Therapeutic Monitoring for Pediatric Brain Tumors

Developing a universal protocol for pediatric brain tumors is a challenge, mainly due to heterogeneous tumor types and tumor components. In general, DWI, perfusion MRI, MRS, and SWI are included in pre-treatment evaluation protocol for pediatric brain tumors. DTI and functional MRI

Table 1. Advanced MRI Findings Helpful to Narrow Differential Diagnosis of Pediatric Brain Tumors

MRI Techniques	Finding	Suggested Tumor
DWI	High ADC value	Necrotic tumor from pyogenic abscess
Perfusion imaging	Low rCBV value	Exclusion of high-grade tumors
	High rCBV value	Atypical teratoid rhabdoid tumor from medulloblastoma
	High rCBV value	Hemangioblastoma from pilocytic astrocytoma
	T1-dominant leakage pattern on DSC imaging	Low-grade tumors
	T2*-dominant leakage pattern with markedly elevated rCBV	Ependymoma and other high-grade tumors
MRS	High Cho/Cr and lower NAA/Cr ratios	High-grade tumors and pilocytic astrocytoma
	NAA:Cho versus Cr:Cho scattergram	Differentiation diagnosis of pediatric cerebellar tumors (35)
	Tau at 3.3 ppm	Medulloblastoma and pediatric supratentorial neuroectodermal tumor
	Elevated mI	Grade II astrocytoma, ependymoma, or choroid plexus papilloma
	Elevated alanine at 1.4–1.5 ppm	Meningioma, glioblastoma, and medulloblastoma
	Acetate (1.9 ppm), succinate (2.4 ppm), and amino acids	Pyogenic abscess
SWI or CT	Calcification	Low-grade tumors

ADC = apparent diffusion coefficient, Cho = choline, Cr = creatine, DSC = dynamic susceptibility contrast, DWI = diffusion-weighted imaging, mI = myoinositol, MRS = MR spectroscopy, NAA = N-acetylaspartate, rCBV = relative cerebral blood volume, SWI = susceptibility-weighted imaging, Tau = taurine

Table 2. Advanced MRI Findings Useful to Monitor Treatment Response in High-Grade Pediatric Brain Tumors

DWI	ADC value or ratio; other quantitative DWI parameters (diffusion kurtosis, diffusion heterogeneity index)
Perfusion imaging	Viable tumor versus radiation necrosis
	True progression versus pseudoprogression
	Particularly helpful after antiangiogenic therapy
MRS	Reduction in high Cho peak suggesting favorable treatment response
	Reduction in citrate peak at 2.6 ppm in brainstem glioma suggesting malignant transformation
	Elevated lipid, low NAA, and low Cho in radiation necrosis

ADC = apparent diffusion coefficient, Cho = choline, DWI = diffusion-weighted imaging, MRS = MR spectroscopy, NAA = N-acetylaspartate

may be performed when the spatial relationship between major white matter tract or eloquent cortical gray matter and tumor needs to be determined before treatment. Pulse sequences with a higher priority should be performed first in the MRI protocol because the attention span for the MRI evaluation in children with brain tumors is often limited. When a tumor contains abundant foci of hemorrhage or calcification, MRS and DSC tend to show low diagnostic yield and may be omitted.

Pulse sequences for post-therapeutic monitoring should also be individualized and imagers should first review imaging findings suggesting viable tumor, such as water diffusion on ADC map and Cho peak on MRS, on pre-treatment MRI (Fig. 9). Of importance, imaging technique should be consistent during longitudinal follow-up studies for the same patient.

CONCLUSION

Probable MRI diagnosis of pediatric brain tumors in clinical practice are usually based on diagnostic clues including tumor location, patient age, clinical history, tumor incidence, and MRI findings. Of importance, advanced brain MRI techniques provide incremental diagnostic value over conventional MRI. However, no single advanced technique is perfect but different techniques typically complement one another. To narrow the differential diagnosis of pediatric brain tumors by using these advanced techniques, identification of findings that are inclusive, exclusive, or highly suggestive is required (Table 1). To monitor treatment response in high-grade tumors accurately, we should be aware of imaging characteristics useful for that purpose (Table 2). Furthermore, functional and pathophysiologic information obtained by advanced brain MRI may provide valuable insights into various imaging phenotypes of pediatric brain tumors and increase the understanding of the link between imaging phenotypes and genotypes. This will become more important with advancement of increasingly individualized and sophisticated management strategies.

REFERENCES

1. Barkovich AJ. *Pediatric Neuroimaging*, 4th ed. Philadelphia, PA: Lippincott Williams & Wilkins, 2005
2. Panigrahy A, Blüml S. Neuroimaging of pediatric brain tumors: from basic to advanced magnetic resonance imaging (MRI). *J Child Neurol* 2009;24:1343-1365
3. Radbruch A, Bendszus M. Advanced MR imaging in neuro-oncology. *Clin Neuroradiol* 2015;25 Suppl 2:143-149
4. Rossi A, Gandolfo C, Morana G, Severino M, Garrè ML, Cama A. New MR sequences (diffusion, perfusion, spectroscopy) in brain tumours. *Pediatr Radiol* 2010;40:999-1009
5. Poretti A, Meoded A, Huisman TA. Neuroimaging of pediatric posterior fossa tumors including review of the literature. *J Magn Reson Imaging* 2012;35:32-47
6. Lacerda S, Law M. Magnetic resonance perfusion and permeability imaging in brain tumors. *Neuroimaging Clin N Am* 2009;19:527-557
7. Romano A, Rossi Espagnet MC, Calabria LF, Coppola V, Figà Talamanca L, Cipriani V, et al. Clinical applications of dynamic susceptibility contrast perfusion-weighted MR imaging in brain tumours. *Radiol Med* 2012;117:445-460
8. Plaza MJ, Borja MJ, Altman N, Saigal G. Conventional and advanced MRI features of pediatric intracranial tumors: posterior fossa and suprasellar tumors. *AJR Am J Roentgenol* 2013;200:1115-1124
9. Borja MJ, Plaza MJ, Altman N, Saigal G. Conventional and advanced MRI features of pediatric intracranial tumors: supratentorial tumors. *AJR Am J Roentgenol* 2013;200:W483-W503
10. Vinogradov E, Sherry AD, Lenkinski RE. CEST: from basic principles to applications, challenges and opportunities. *J Magn Reson* 2013;229:155-172
11. Goo HW. High field strength magnetic resonance imaging in children. *J Korean Med Assoc* 2010;53:1093-1102
12. Lam WW, Poon WS, Metreweli C. Diffusion MR imaging in glioma: does it have any role in the pre-operation determination of grading of glioma? *Clin Radiol* 2002;57:219-225
13. Porto L, Jurcoane A, Schwabe D, Kieslich M, Hattingen E. Differentiation between high and low grade tumours in paediatric patients by using apparent diffusion coefficients. *Eur J Paediatr Neurol* 2013;17:302-307
14. Gimi B, Cederberg K, Derinkuyu B, Gargan L, Koral KM, Bowers DC, et al. Utility of apparent diffusion coefficient ratios in distinguishing common pediatric cerebellar tumors. *Acad Radiol* 2012;19:794-800
15. Bull JG, Saunders DE, Clark CA. Discrimination of paediatric brain tumours using apparent diffusion coefficient histograms. *Eur Radiol* 2012;22:447-457
16. Bai Y, Lin Y, Tian J, Shi D, Cheng J, Haacke EM, et al. Grading of gliomas by using monoexponential, biexponential, and stretched exponential diffusion-weighted MR imaging and diffusion kurtosis MR imaging. *Radiology* 2016;278:496-504
17. Sui Y, Wang H, Liu G, Damen FW, Wanamaker C, Li Y, et al. Differentiation of low- and high-grade pediatric brain tumors with high b-value diffusion-weighted MR imaging and a fractional order calculus model. *Radiology* 2015;277:489-496
18. Jellison BJ, Field AS, Medow J, Lazar M, Salamat MS, Alexander AL. Diffusion tensor imaging of cerebral white matter: a pictorial review of physics, fiber tract anatomy, and tumor imaging patterns. *AJNR Am J Neuroradiol* 2004;25:356-369

19. Lu S, Ahn D, Johnson G, Law M, Zagzag D, Grossman RI. Diffusion-tensor MR imaging of intracranial neoplasia and associated peritumoral edema: introduction of the tumor infiltration index. *Radiology* 2004;232:221-228
20. Leclercq D, Delmaire C, de Champfleur NM, Chiras J, Lehéricy S. Diffusion tractography: methods, validation and applications in patients with neurosurgical lesions. *Neurosurg Clin N Am* 2011;22:253-268, ix
21. Lee SK. Diffusion tensor and perfusion imaging of brain tumors in high-field MR imaging. *Neuroimaging Clin N Am* 2012;22:123-134, ix
22. Khong PL, Kwong DL, Chan GC, Sham JS, Chan FL, Ooi GC. Diffusion-tensor imaging for the detection and quantification of treatment-induced white matter injury in children with medulloblastoma: a pilot study. *AJNR Am J Neuroradiol* 2003;24:734-740
23. Fandino J, Kollias SS, Wieser HG, Valavanis A, Yonekawa Y. Intraoperative validation of functional magnetic resonance imaging and cortical reorganization patterns in patients with brain tumors involving the primary motor cortex. *J Neurosurg* 1999;91:238-250
24. O'Shaughnessy ES, Berl MM, Moore EN, Gaillard WD. Pediatric functional magnetic resonance imaging (fMRI): issues and applications. *J Child Neurol* 2008;23:791-801
25. Ogg RJ, Laningham FH, Clarke D, Einhaus S, Zou P, Tobias ME, et al. Passive range of motion functional magnetic resonance imaging localizing sensorimotor cortex in sedated children. *J Neurosurg Pediatr* 2009;4:317-322
26. Kokkonen SM, Nikkinen J, Remes J, Kantola J, Starck T, Haapea M, et al. Preoperative localization of the sensorimotor area using independent component analysis of resting-state fMRI. *Magn Reson Imaging* 2009;27:733-740
27. Jahng GH, Li KL, Ostergaard L, Calamante F. Perfusion magnetic resonance imaging: a comprehensive update on principles and techniques. *Korean J Radiol* 2014;15:554-577
28. Thompson EM, Guillaume DJ, Dósa E, Li X, Nazemi KJ, Gahramanov S, et al. Dual contrast perfusion MRI in a single imaging session for assessment of pediatric brain tumors. *J Neurooncol* 2012;109:105-114
29. Kanda T, Ishii K, Kawaguchi H, Kitajima K, Takenaka D. High signal intensity in the dentate nucleus and globus pallidus on unenhanced T1-weighted MR images: relationship with increasing cumulative dose of a gadolinium-based contrast material. *Radiology* 2014;270:834-841
30. Stojanov D, Aracki-Trenkic A, Benedeto-Stojanov D. Gadolinium deposition within the dentate nucleus and globus pallidus after repeated administrations of gadolinium-based contrast agents-current status. *Neuroradiology* 2016;58:433-441
31. Ho CY, Cardinal JS, Kamer AP, Kralik SF. Relative cerebral blood volume from dynamic susceptibility contrast perfusion in the grading of pediatric primary brain tumors. *Neuroradiology* 2015;57:299-306
32. Cho SK, Na DG, Ryoo JW, Roh HG, Moon CH, Byun HS, et al. Perfusion MR imaging: clinical utility for the differential diagnosis of various brain tumors. *Korean J Radiol* 2002;3:171-179
33. Ho CY, Cardinal JS, Kamer AP, Lin C, Kralik SF. Contrast leakage patterns from dynamic susceptibility contrast perfusion MRI in the grading of primary pediatric brain tumors. *AJNR Am J Neuroradiol* 2016;37:544-551
34. Goo HW, Ra YS. Medullary hemangioblastoma in a child with von Hippel-Lindau disease: vascular tumor perfusion depicted by arterial spin labeling and dynamic contrast-enhanced imaging. *J Neurosurg Pediatr* 2015;16:50-53
35. Hales PW, Phipps KP, Kaur R, Clark CA. A two-stage model for in vivo assessment of brain tumor perfusion and abnormal vascular structure using arterial spin labeling. *PLoS One* 2013;8:e75717
36. White CM, Pope WB, Zaw T, Qiao J, Naeini KM, Lai A, et al. Regional and voxel-wise comparisons of blood flow measurements between dynamic susceptibility contrast magnetic resonance imaging (DSC-MRI) and arterial spin labeling (ASL) in brain tumors. *J Neuroimaging* 2014;24:23-30
37. Yeom KW, Mitchell LA, Lober RM, Barnes PD, Vogel H, Fisher PG, et al. Arterial spin-labeled perfusion of pediatric brain tumors. *AJNR Am J Neuroradiol* 2014;35:395-401
38. Brandão LA, Poussaint TY. Pediatric brain tumors. *Neuroimaging Clin N Am* 2013;23:499-525
39. Wang Z, Sutton LN, Cnaan A, Haselgrove JC, Rorke LB, Zhao H, et al. Proton MR spectroscopy of pediatric cerebellar tumors. *AJNR Am J Neuroradiol* 1995;16:1821-1833
40. Shiroishi MS, Panigrahy A, Moore KR, Nelson MD Jr, Gilles FH, Gonzalez-Gomez I, et al. Combined MRI and MRS improves pre-therapeutic diagnoses of pediatric brain tumors over MRI alone. *Neuroradiology* 2015;57:951-956
41. Löbel U, Sedlacik J, Sabin ND, Kocak M, Broniscer A, Hillenbrand CM, et al. Three-dimensional susceptibility-weighted imaging and two-dimensional T2*-weighted gradient-echo imaging of intratumoral hemorrhages in pediatric diffuse intrinsic pontine glioma. *Neuroradiology* 2010;52:1167-1177
42. Tong KA, Ashwal S, Obenaus A, Nickerson JP, Kido D, Haacke EM. Susceptibility-weighted MR imaging: a review of clinical applications in children. *AJNR Am J Neuroradiol* 2008;29:9-17
43. Di Ieva A, Lam T, Alcaide-Leon P, Bharatha A, Montanera W, Cusimano MD. Magnetic resonance susceptibility weighted imaging in neurosurgery: current applications and future perspectives. *J Neurosurg* 2015;123:1463-1475
44. Togao O, Yoshiura T, Keupp J, Hiwatashi A, Yamashita K, Kikuchi K, et al. Amide proton transfer imaging of adult diffuse gliomas: correlation with histopathological grades. *Neuro Oncol* 2014;16:441-448
45. Sagiyama K, Mashimo T, Togao O, Vemireddy V, Hatanpaa KJ, Maher EA, et al. In vivo chemical exchange saturation transfer imaging allows early detection of a therapeutic response in glioblastoma. *Proc Natl Acad Sci U S A* 2014;111:4542-4547